Combined Manganese Oxides as Oxygen Carriers for Biomass Combustion – Ash Interactions

Ivana Staničić[1*], Viktor Andersson[2], Malin Hanning[1], Tobias Mattisson[1], Rainer Backman[3], Henrik Leion[4]

[1] *Department of Space, Earth and Environment, Division of Energy Technology, Chalmers University of Technology, SE-412 96 Gothenburg, Sweden*

[2] *Department of Chemistry and Molecular Biology, Atmospheric Science, University of Gothenburg, SE-412 96 Gothenburg, Sweden*

[3] *Department of Applied Physics and Electronics, Thermochemical Energy Conversion Laboratory, Umeå University, SE 901 87 Umeå, Sweden*

[4]*Department of Chemistry and Chemical Engineering, Chalmers University of Technology, SE-412 96 Gothenburg, Sweden*

[*]*stanicic@chalmers.se*

Abstract

Carbon capture and storage (CCS) has been acknowledged as an important strategy for mitigation of climate change. Although highly applicable for fossil fuels, CCS with biomass could have the added advantage of resulting in negative emissions of carbon dioxide. One promising carbon capture technology is chemical-looping combustion (CLC). In CLC the reactors are filled with metal oxide bed material called oxygen carriers. Before CLC can be implemented for biomass combustion at a large scale, biomass ash components interaction with oxygen carriers needs to be further understood.

Four combined manganese combined oxides, $(Mn_3O_4)_{3.8}$-SiO_2, $(Mn_3O_4)_{5.8}$-$(SiO_2)_{1.5}$-TiO_2, $(Mn_3O_4)_2$-$Fe_2O_3$and Mn_3O_4-$(Fe_2O_3)_{2.2}$-$(Al_3O_4)_{1.1}$ were exposed to common biomass ash components K, Ca and P. The ash components can exist in many forms, but here the compounds $CaCO_3$, K_2CO_3 and $CaHPO_4$ were used. Exposures were performed at 900°C for six hours in oxidising, reducing and inert conditions. Crystalline phases were analysed by XRD and morphology examined with SEM-EDX.

Results show that oxygen carrier particles containing silicon were more likely to form agglomerates, especially in combination with potassium, whereas the particles including iron were more stable. MnFeAl was the oxygen carrier that showed least agglomerating behaviour while simultaneously showing a propensity to absorb some ash components.

Some inconsistencies between thermodynamic predictions and experimental results is observed. This may be explained by lack of relevant data in the used databases, were only a few of the oxygen carrier-ash systems and subsystems have been optimised. Further optimisation related to manganese rich systems should be performed to obtain reliable results.

1. Introduction

The Paris Agreement, imposed in 2015, specifies that the increase in the global average temperature should be limited to below 2°C, and that efforts should be pursued to limit the increase to 1.5°C. To meet this target, emissions of the greenhouse gases would need to be reduced to almost zero in less than twenty years. It is plausible that active removal of carbon dioxide from the atmosphere will become necessary [1]. Carbon capture and storage (CCS) has been acknowledged as an important strategy for mitigation of climate change [2]. This technology could be applied to all types of fuels, including fossil fuel, biomass or waste. Although highly applicable for fossil fuels, CCS with biomass could have the added advantage of resulting in negative emissions of carbon dioxide. Bioenergy with carbon capture and storage (BECCS) is regarded as the most efficient way to reach climate targets [3, 4]. One promising carbon capture technology is chemical-looping combustion (CLC), which avoids the costly and energy intensive gas-gas separation needed in other capture technologies. This is possible by using metal oxides with the ability to be oxidised or reduced at combustion conditions depending on the surrounding oxygen partial pressure. Numerous metal oxides, referred to as oxygen carriers, have been operated in chemical-looping units ranging from small lab-scale units up to a 1 MW_{th} reactor unit [5, 6].

A common way to realise chemical-looping combustion is by using two interconnected fluidised bed reactors. The reactors are filled with bed material called oxygen carriers. The oxygen carriers have the form of small particles of a suitable size range and is circulated between the two reactors. It is reduced in the fuel reactor and oxidised in the air reactor. By using this method, knowledge and experience of combustion in circulating fluidised bed (CFB) boilers can be used. Most chemical-looping pilot units today uses interconnected fluidised beds as a way to transport material [7].

In combustion of a solid fuel, gaseous volatiles will first be released in the fuel reactor, and subsequently react directly with the oxygen carrier. The remaining char needs to be gasified with steam or carbon dioxide to be able to react with the oxygen carrier in a gas-solid reaction. Char gasification with steam as oxidising agent is rather slow compared to the other combustion reactions and it would therefore be the rate limiting factor for the conversion of the char [8]. This could be problematic since a long fuel residence time of the solids may be needed to reach complete burnout of the fuel.

The choice of oxygen carrier offers a way around the slow char gasification step. Some metal oxides are capable of releasing oxygen directly in gaseous form at temperatures relevant for fuel combustion. The char can then react directly with the gaseous oxygen released from the oxygen carrier and will not need to be gasified first. This combustion scheme is referred to as chemical-looping with oxygen uncoupling (CLOU) [9]. CLOU also allows for a gas-gas reaction between oxygen and volatiles, instead of a gas-solid reaction which requires good contact. This implies that CLOU can facilitate complete combustion even though the mixing between oxygen carrier and fuel is inadequate.

1.1. Combined Manganese Oxides as Oxygen Carriers

Manganese, cobalt, copper and iron form oxides with oxygen releasing properties at combustion conditions. The equilibrium oxygen partial pressure is shown as a function of temperature for these oxides in Figure 1. The equilibrium partial pressure of oxygen is not only decisive for the oxygen release in the fuel reactor, but it also determines the driving force for oxidation in the air reactor. The equilibrium partial pressure should be low enough for oxidation to occur at a reasonable oxygen concentration. A high partial pressure of oxygen in the outlet from the air reactor corresponds to operating with a high air-to-fuel ratio which generates a high heat loss associated with the flue gases. Normally employed air-to-fuel ratios correspond to an outlet concentration of oxygen at around 5 vol.%. Consequently, the equilibrium partial pressure of oxygen needs to be below this level at the chosen air reactor temperature for oxidation to occur throughout the entire reactor volume.

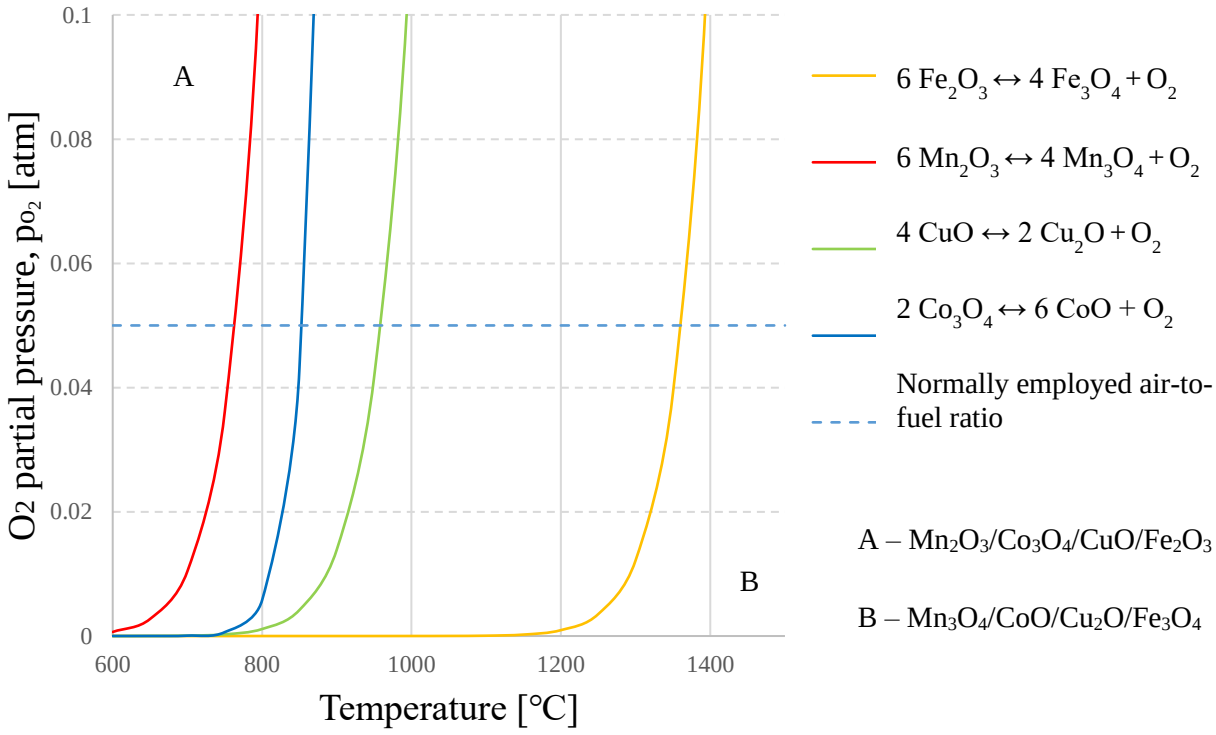

Figure 1 Equilibrium oxygen partial pressure of manganese, cobalt, copper and iron oxides and their corresponding phase transition reactions.

Manganese oxides can release gaseous oxygen, but the relevant equilibrium concentrations occur below 800°C, see Figure 1, and re-oxidation of the material is slow at this temperature [9]. However, the thermodynamic properties of manganese oxides can be altered by combining manganese with other metals such as iron, silicon, calcium, nickel, magnesium and copper [10]. Combined oxides of manganese-iron, manganese-nickel and manganese-silica were investigated in a fluidised batch reactor. The combined manganese-iron oxygen carrier was shown to have oxygen release properties and high reactivity with methane [11]. Later research has focused more on combined oxides of Mn-Fe, Mn-Si and Mn-Fe-Si. These systems have the ability to release oxygen and have all shown promising results [12-18].

1.2. Biomass Ash in Fluidised Beds

Biomass ashes are highly reactive and known to interact with bed materials in fluidised bed combustion [19-22]. This could result in agglomeration of the bed material and hamper operation. Further, volatile organics could also act as precursors for high-temperature corrosion phenomena. Agglomerations are usually caused by the reaction of alkali with silica, forming alkali silicates. These have low melting temperatures and therefore tend to form agglomerates [19, 23, 24]. Potassium is most often the main alkali source in biomass ashes. Potassium may also react with chlorine, forming gaseous potassium chloride. This compound follows the flue gases into the convection path of the boiler where it can cause problems such as corrosion and fouling [22]. The formation of gaseous alkali chloride compounds also promotes the reaction of alkali with silicates due to the increased mobility of alkali [19]. The alkali balance in the boiler and its effects on the operation, is affected by the interaction between these species and the bed material. Using bed materials other than the commonly used silica sand may reduce the tendency for agglomeration [25]. On the other hand this could result in increased concentrations of alkali in the gas phase, increasing the problems related to deposition of alkali on down-stream on heat-transfer surfaces as more alkali will leave the bed in gaseous form.

In chemical-looping, the bed consists of an oxygen carrier which needs to transfer oxygen continuously in an alternating oxidising and reducing atmosphere. Hence, any ash interaction could have additional effects besides bed agglomeration. Ash components at the surface or in the bulk of the oxygen carrier may alter the reaction kinetics of the oxygen carrier. The reaction rate can be decreased if gas diffusion is hindered by an ash layer formed on the surface of the particles. Attached ash components on the carrier could on the other hand have a catalysing effect on the reaction or even have oxygen carrier properties in itself [26]. Ash components reacting with the oxygen carrier and altering the composition could either increase or decrease the oxygen transport capacity and rate depending on the compounds formed.

There are several publications on interactions between ash and oxygen carriers, but most concern coal ash components [27-34]. However, there are some studies on interactions between biomass ash and iron-based oxygen carriers [23, 35, 36]. For example, Gu et al investigated the interaction between iron ore and three different biomasses (corn stalk, rape stalk and wheat straw) [23]. The study was conducted in a lab-scaled fixed bed. The bed material was collected and analysed with XRD, BET, SEM-EDX and XRF. The study showed that silica rich ash produced molten potassium silicates while potassium rich ash, with less silica, improved the reactivity of the oxygen carriers [23]. Corcoran et al. investigated the physical and chemical changes of the natural ore ilmenite during combustion with biomass [35]. The samples were analysed using SEM-EDX and XRD. Some samples were also analysed by XRF and ICP-OES and leaching experiments were performed to evaluate the capability of extracting soluble ash compounds. Results show that iron segregated to the surface and enrichment of titanium was found in the particle core. Calcium was found to form a layer on the particle, while potassium diffused into the particles forming KTi_8O_{16}. Leaching experiments showed that both calcium and potassium were leachable to a limited degree [35].

1.3. Aim of Study

The way that biomass ash components interact with oxygen carriers needs to be further understood before CLC can be implemented for biomass combustion at a large scale. In this study, four previously developed manganese-based oxygen carriers are investigated with respect to their interaction with biomass ash. Solids plus ash components were exposed to high temperature and variable gas atmospheres. The purpose is to examine whether new compounds are formed as a result of interaction between oxygen carrier and ash elements. This can be regarded as a first step in acquiring a deeper knowledge of how combined manganese oxides would perform as bed material in the presence of biomass ash. For complete understanding, experimental results were compared with results from multicomponent modelling using FactSage with the FToxid-database.

2. Experimental

2.1. Material

Four manganese-based oxygen carriers have been included in the study, namely oxides in the system Mn-Si, Mn-Si-Ti, Mn-Fe and Mn-Fe-Al. All materials have previously been tested as oxygen carriers and showed promise. [12, 37-39] The materials were produced by VITO, an independent research organisation in Belgium. The oxygen carriers were produced by spray drying and thereafter sieving to obtain the right size range. To have sufficient mechanical strength sintering was performed in air for four hours, after which they were sieved again to the size range of 125-180μm. Properties of the fresh materials are presented in Table 1.

Table 1 Properties and sintering temperatures of fresh materials.

Material	MnSi	MnSiTi	MnFe	MnFeAl
Synthesis composition (wt%)	75% Mn_3O_4, 25% SiO_2	66.7% Mn_3O_4 22.3% SiO_2 11.0% TiO_2	32.3% Mn_3O_4 67.7% Fe_2O_3	20.5% Mn_3O_4 42.9% Fe_2O_3 36.6% AlOOH
Molar ratio	Mn:Si=2.4	Mn:Si=2.4 Ti:(Mn+Si)=0.1	Mn:Fe=0.5	Mn:Fe=0.5 Al:(Mn+Fe)=0.757
Bulk density (g/cm^3)	1.0	1.7	1.6	1.2
Mean particle size (μm)	136	126	153	153
Crushing strength (N)	0.5	2.1	0.9	0.9
Sintering temperature (°C)	1150	1140	1100	1100
Previously tested in	[37]	[37]	[12, 38]	[39]

This study investigates three common ash elements which could be important for different types of biomass, and which are known to be important precursors for melts and reactive at high temperatures; potassium, calcium and phosphorous [40]. These elements are not encountered in pure form in the ash, but rather as different compounds and could be present in both gas, liquid or solid phase in the combustion chamber. The release mechanism from the fuel during conversion could be quite complicated and depends upon temperature, fuel type, gas surroundings and other factors [41]. It was decided to focus on a few simple solid compounds which include the main reactive ash element. In this way it is believed that the

relative propensity to react will be determined. Thus, the following contaminants were used to represent the ash components; K_2CO_3, $CaCO_3$ and $CaHPO_4$, each a fine powder with a purity above 99.9% provided by Sigma-Aldrich.

2.2. Exposure Procedure

The exposure was carried out in an alumina fixed bed tubular furnace manufactured by Vecstar together with a tubular quartz reactor. Temperature profile was obtained in the furnace to position the samples correctly.

The interactions between oxygen carrier and ash compound were investigated in three different environments. Each environment corresponds to a section in the CLC process. The oxidising environment models the air reactor, reducing environment the fuel reactor and inert the particle seals located between the reactors, which may be fluidised with an inert compound. In total, 36 exposure experiments were performed at atmospheric pressure.

The total gas flow through the tube was kept at 140 ml/min which was controlled by a needle valve. Pure nitrogen gas was used for the inert environment while oxidising environment consisted of synthetic air with 21 vol.% O_2 and 79 vol.% N_2. To avoid complete reduction of the oxygen carriers and to better mimic the fuel reactor, steam was mixed with hydrogen. Therefore, the reducing conditions consisted of 2.5 vol.% H_2, 47.5 vol.% Ar and 50 vol.% H_2O, which results in a reducing potential, pH_2/pH_2O of 0.05. This corresponds to an equilibrium partial pressure of O_2 of $\log_{10}p(O_2)$ of -13.7 atm.

An equal amount of oxygen carrier and ash compound with a total weight of 5g was manually mixed in a small container by shaking. Ceramic boats were used as sample holders and a marked steel rod was used to position the sample in the furnace. After positioning the samples, the furnace was turned on and samples exposed to one of the three environments. For oxidising and inert conditions gas was turned on during warm-up where temperature increased with a rate of 10°C/min. For reducing conditions nitrogen gas was used until 900°C was reached. When the furnace reached this temperature the steam flow was first turned on, followed by the hydrogen in argon and lastly the nitrogen gas was turned off. Six hours after reaching 900°C the gas and the furnace were turned off and sample left to cool inside the furnace. For the reducing and inert environment nitrogen was turned on during the cooling process while oxidising exposure was cooled down in air. The samples were cooled down to room temperature for approximately 12 hours in inert environment.

2.3. Characterisation

Samples were pre-treated by light crushing in a mortar before crystalline phases were determined by x-ray powder diffraction (XRD). For this purpose, the Bruker D8 Advanced system was used with $CuK_{\alpha 1}$ radiation. The diffractometer was collected at angles of 20-80º.

Morphology was examined by a scanning electron microscope (SEM-EDX) and distribution of elements in the particles were also studied for samples which showed indications of interaction. This analysis did not require any specific sample preparation unless the samples formed hard compounds after exposure. These needed to be pre-treated by light crushing in a mortar. For this analysis Quanta 200 ESEM FEG from FEI was used. This system is equipped with an Oxford Inca Energy Dispersive X-ray (EDX) system for chemical analysis. Cross

section analysis was performed on some samples. For this specific investigation, the samples had to be prepared by moulding the sample into epoxy. This was done by mixing resin and hardener with a weight ratio of 25:3. The samples were then placed in a silicone covered cup, covered with the mixture and placed in vacuum until hardened. Samples were then polished maximum 30 minutes before analysing the cross section of the particles.

2.4. Thermodynamic Calculation

Thermodynamic calculations were performed to predict which compounds could be formed in the experiments. This was done by FactSage 7.2®, a common computational aid for this purpose. This is an integrated database computing system. It consists of calculation and manipulation modules that can access many different solution databases and substances. FactSage 7.2® databases have been developed by optimising literature data. The program includes many modules which allows calculations of conditions for multiphase, multicomponent equilibrium and phase diagrams. The module *Equilib* was used for the thermodynamic equilibrium calculations in this study. The module requires inputs of reactants and conditions such as temperature, total pressure and partial pressures if needed. Possible product phases and solution databases also need to be specified. Thereafter Gibbs energy minimisation principle is used to calculate the amount of each product at chemical equilibrium state.

A sample of 2.5g of oxygen carrier and 2.5g of ash component were recalculated to molar basis and defined in FactSage 7.2®. The composition of the gaseous phase is the same as that flowing through the tubular reactor. The gaseous components were introduced in large excess in the calculation, hence maintaining a relatively constant partial pressure of oxygen around the particles. Two different databases are included in this study. The databases FactPS for pure solids and FToxid for all pure oxides and oxide solutions were used. All solution phases were included in the calculations. Among the compounds found in the solution phase FT-Slag, the pure liquid compound species were neglected. This was done to allow the slag phase to form which is more likely compared to the liquid. As the ash components are heated to 900°C, the carbonates will form the oxides CaO, K_2O and $Ca_2P_2O_7$. Therefore, these compounds were used for calculations of phase diagrams, as it is not expected that carbon will be present.

3. Results

Results have been summarised in three tables below, one table summarising the results for each ash component. The tables contain information for exposure with oxygen carrier and environment. Crystalline phases have been identified with XRD using powder diffraction file (PDF) databases provided by ICDD (International Centre for Diffraction Data). These reference patterns are used to recognize chemical phases measured and each phase has a unique PDF-number. These numbers are defined in the tables.

Compounds found by FactSage are presented for each exposure in order of decreasing concentration. Phases are indicated in the table as solid (s), solid solution (ss) and slag (slag) phase. A solid solution is formed when a mixture of two or more crystalline solids coexist as a new crystalline solid or crystalline lattice. Each solid solution is indicated in the table with a

number i.e. ss1, ss2... Ash components forming gaseous compound are also indicated in the table as (g). Compounds formed below 10^{-5} moles were excluded from the table.

Before exposure each oxygen carrier was examined under electron microscope. Hollow spaces for both MnFe and MnFeAl can be observed. This is a result from the production procedure. If ash compounds are much smaller there is a possibility that they may accumulate inside this hollow space.

3.1. Interactions with calcium carbonate

Results for exposures including calcium carbonate are gathered in Table 2. The table gives an overview of the XRD and FactSage results as well as the visual observation of the sample after exposure.

Table 2 Summarised results for exposures carried out with calcium carbonate. Interaction between ash and oxygen carrier in italic and bold text.

Oxygen carrier		**XRD**		**FactSage**		**Visual**
		Compound	**PDF No**			
MnSi	Oxidising	***$CaSiO_3$***	00-066-0271	SiO_2	(s)	Grey-white powder
		Mn_7SiO_{12}	00-033-0904	Mn_7SiO_{12}	(ss1)	
		$CaMn_{14}SiO_{24}$	00-041-1363	***$CaSiO_3$***	(ss2)	
		CaO	00-043-1001	Mn_8O_{12}	(ss1)	
		SiO_2	01-079-0446	$MnSiO_3$	(ss2)	
	Reducing	CaO	00-043-1001	Mn_2SiO_4	(ss1)	Grey-white powder
		$CaMn_{14}SiO_{24}$	00-041-1363	MnO	(ss2)	
		Mn_7SiO_{12}	00-033-0904	***$CaMnSiO_4$***	(ss1)	
		$MnSiO_3$	04-013-3697	***Ca_2SiO_4***	(ss1)	
				CaO	(ss2)	
	Inert	Mn_7SiO_{12}	00-043-1001	$MnSiO_3$	(ss1)	Grey-white powder
		CaO	00-033-0904	Mn_7SiO_{12}	(ss2)	
		SiO_2	00-046-1045	SiO_2	(s)	
				$CaSiO_3$	(ss1)	
				Mn_8O_{12}	(ss2)	
MnSiTi	Oxidising	CaO	00-043-1001	SiO_2	(s)	Grey-white powder
		$CaTiO_3$	04-018-8646	TiO_2	(ss1)	
		$CaSiO_3$	00-066-0271	Mn_7SiO_{12}	(ss2)	
		$MnSiO_3$	04-013-3697	***$CaSiO_3$***	(ss3)	
		Mn_7SiO_{12}	00-033-0904	$MnSiO_3$	(ss3)	
		Mn_2O_3	04-005-4578	Mn_8O_{12}	(ss2)	
	Reducing	***$CaMn_{14}SiO_{24}$***	00-041-1368	Mn_2SiO_4	(ss1)	Grey-white powder
		CaO	04-043-1001	$MnTiO_3$	(ss2)	
		Mn_2SiO_4	04-007-9023	***$CaMnSiO_4$***	(ss1)	
		TiO_2	04-011-0664	$MnTi_2O_4^{2+}$	(ss3)	
					(ss3)	

				$Mn_3O_4^{2-}$ ***Ca_2SiO_4***	(ss1)	
	Inert	TiO_2 ***Ca_2SiO_4*** $MnSiO_3$ ***$CaTiO_3$*** Mn_2O_3 CaO	04-005-4661 00-023-1043 04-013-3698 04-018-8646 04-005-4578 04-043-1001	***Ca_2SiO_4*** $Mn_3O_4^{()(+)(2-)(-)}$ ***$Ca_3Ti_2O_7$*** CaO MnO Mn_2SiO_4	(ss1) (ss2) (s) (ss3) (ss3) (ss1)	Grey-white powder
MnFe	Oxidising	CaO Mn_2O_3 $Mn_{0.983}Fe_{0.017}O_3$ ***$CaFe_2O_4$***	00-043-1001 04-005-4578 00-024-0507 00-003-0040	***$Ca_2Fe_2O_5$*** CaO $Mn_3O_4^{()(+)(2-)(+)(-)}$ MnO $Fe_2MnO_4^{()(+)}$ $FeMn_2O_4^{(+)(-)}$ Fe_2O_3	(s) (ss1) (ss2) (ss1) (ss2) (ss2) (ss1)	Dark grey, powder
	Reducing	CaO ***$Ca_2Mn_{0.2}Fe_{1.8}O_5$*** $(FeO)_{0.198}(MnO)_{0.802}$ ***$(CaO)_{0.9}(MnO)_{0.1}$*** ***$Ca_2Fe_2O_5$***	00-037-1497 04-006-9168 01-077-2361 00-036-1378 04-006-8401	MnO ***$Ca_2Fe_2O_5$*** CaO FeO Fe_2O_3	(ss1) (s) (ss1) (ss1) (ss1)	Dark brown powder
	Inert	CaO Fe_2O_3 ***$Ca_2Fe_2O_5$*** Mn_2O_3 MnO	00-043-1001 00-039-0238 04-006-8401 04-005-4578 00-006-0592	***$Ca_2Fe_2O_5$*** CaO $Mn_3O_4^{()(+)(2-)(-)}$ MnO $FeMn_2O_4^{(+)(-)}$ Fe_2O_3	(s) (ss1) (ss2) (ss1) (ss2) (ss1)	Grey-white powder
MnFeAl	Oxidising	CaO $MnFeO_3$ Fe_2O_3 $MnFeAlO_4$ ***$Ca_2Fe_2O_5$*** ***$Ca_{0.55}Al_{11}O_{17.05}$*** Mn_2O_3 Al_2O_3	00-043-1001 04-015-4711 00-039-1346 04-005-9715 04-006-8401 00-048-0501 04-005-4578 00-056-1186	Mn_2O_3 ***$Ca_2Fe_2O_5$*** ***$CaAl_4O_7$*** ***$CaAl_2O_4$*** Fe_2O_3 ***$Ca_2Al_2O_5$*** ***$CaFe_4O_7$*** ***$CaFe_2O_4$*** Al_2O_3	(ss1) (ss2) (ss3) (ss4) (ss1) (ss2) (ss3) (ss4) (ss1)	Grey-white powder
	Reducing	$Fe_{2.02}Mn_{0.98}O_4$ Mn_2AlO_4 Fe_2O_3 **$Ca_2Fe_2O_5$** **$Ca_2Al_{1.38}Fe_{0.62}O_5$** CaO	01-078-6782 00-029-0881 00-039-1346 04-006-8401 00-042-1469 00-043-1001	***$CaAl_2O_4$*** MnO ***$Ca_2Fe_2O_5$*** ***$Ca_2Al_2O_5$*** FeO ***$CaFe_2O_4$*** CaO Fe_2O_3	(ss1) (ss2) (ss3) (ss3) (ss2) (ss1) (ss2) (ss2)	Dark brown powder

				Al_2O_3	(ss2)	
	Inert	CaO	00-043-1001	$MnAl_2O_4$	(ss1)	Grey-white powder
		Fe_3O_4	04-007-2412	***$Ca_2Fe_2O_5$***	(ss2)	
		Mn_2AlO_4	00-029-0881	***$Ca_2Al_2O_5$***	(ss2)	
		Al_2O_3	00-010-0173	$FeAl_2O_4$	(ss1)	
				MnO	(ss3)	
				FeO	(ss3)	
				Fe_2O_3	(ss3)	
				CaO	(ss3)	
				Al_2O_3	(ss3)	

3.1.1. Phase Composition

Visually the samples did not change drastically after exposure. Some samples had slight colour change but were still powders after exposure. XRD showed that three interacted compounds were formed for MnSi summarised over all investigated environments. The other oxygen carriers formed five interacted compounds for MnSiTi, five for MnFe and four for MnFeAl.

For each combination of oxygen carrier and environment, the appearance was similar to those shown in Figure 2, which shows SEM-EDX images for the cross section of MnFe and MnSiTi after exposure in reducing environment. Figure 2 (top left) shows two oxygen carriers surrounded by smaller particles. An empty space in the middle of these oxygen carriers can be identified. Mapping of calcium (top and bottom right) show that the space occupied by the

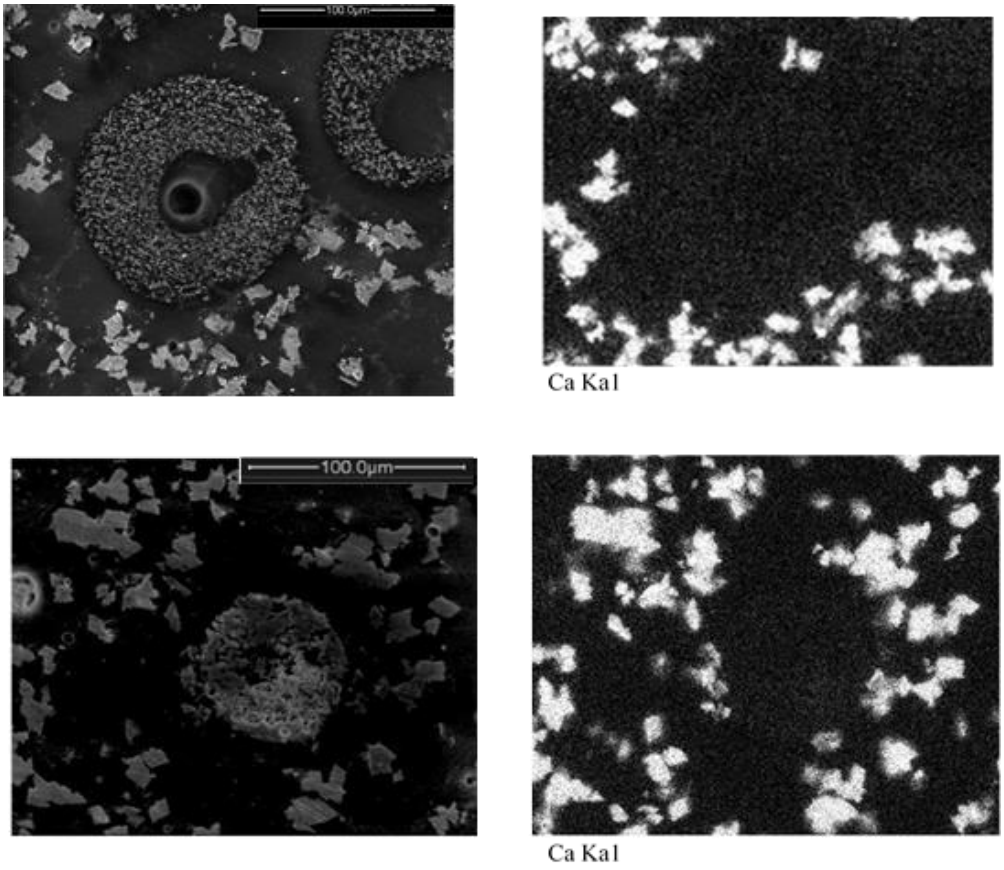

Figure 2 Cross section analysis after exposure in reducing environment with calcium carbonate and oxygen carriers MnFe (top) and MnSiTi (bottom). Electron image to the left and element mapping of calcium to the right.

oxygen carrier particles are empty and that no penetration of calcium occurs. Except for some ash particles sticking to the oxygen carrier surfaces, samples exposed with calcium carbonate did not show any agglomerating behaviour in any investigated case. Clusters of particles were not detected, and individual oxygen carriers were found all over the analysed samples.

From Table 2 XRD results show that CaO was found in every case. Interaction with manganese and silicon was found forming $CaSiMn_{14}O_{24}$ for MnSi and MnSiTi in reducing environment. Additionally, Table 2 shows that $Ca_2Fe_2O_5$ was formed for MnFe and MnFeAl in reducing environment. Original structures, such as Fe_2O_3, Mn_2O_3, TiO_2 and SiO_2 were also found by XRD in many cases indicating no significant change of the main compounds included in the manufacturing. Even though interacted compounds were found all samples were still powders after exposure with no significant colour changes. Least interacted compounds were found in samples exposed to the inert environment while both the reducing and oxidising exposures resulted in similar degree of interactions.

3.1.2. Thermodynamic Calculations

In general, thermodynamic calculations showed formation of phases including species from both ash and oxygen carrier in all investigated cases. Calculations for MnSi predicted three interacted compounds in total for all investigated environments. The other oxygen carriers formed four for MnSiTi, three for MnFe and six for MnFeAl. These results may depend on the

comprehensiveness of databases used. More interacted compounds present does not necessarily indicate agglomeration although it may contribute, thus SEM-EDX images are necessary to detect whether particles have formed clusters. Although the correlation of compounds/phases between XRD and thermodynamic calculation was not exact, both indicated presence of pure compounds and mixed oxides. The largest difference was found for MnFe and MnFeAl. For MnFe two additional compounds were found by XRD. Formation of $(CaO)_{0.9}(MnO)_{0.1}$ was detected in reducing environment which is indirectly accounted for by FactSage through formation of CaO and MnO (ss1) in one phase. For MnFeAl on the other hand, two additional compounds were predicted by calculations. It is possible that a small amount was formed during exposure becoming non-detectable by XRD.

One compound found by the thermodynamic calculation is $MnCaSiO_4$ while XRD found $CaMn_{14}SiO_{24}$ for both MnSi and MnSiTi. This difference may be due to lack of information. For example, databases used for evaluating the diffractograms or even FactSage databases may lack some compounds. Non-compatibility of these two databases may also be a source for this mismatch.

3.2. Interactions with potassium carbonate

Results for exposures including potassium carbonate are gathered in Table 3. The table gives an overview of the XRD and FactSage results as well as the visual observation of the sample after exposure.

Table 3 Summarised results for exposures carried out with potassium carbonate. Interaction between ash and oxygen carrier in italic and bold text.

Oxygen carrier		**XRD**		**FactSage**		**Visual**
		Compound	**PDF No**			
MnSi	Oxidising	***$K_2Si_4O_9$***	04-011-6870	$Mn_3O_4^{()(+)(2-)}$	(ss1)	Black Stone-hard
		K_2MnO_4	04-010-3595	***$K_2Si_2O_5$***	(s)	
		$K_{1.03}Mn_2O_4$	01-080-7316	SiO_2	(slag)	
		SiO_2	01-079-0446	K_2O	(slag)	
		Mn_3O_4	00-024-0734	MnO	(slag)	
	Reducing	***$K_2Si_4O_9$***	04-010-7078	MnO	(ss1)	Green and black. Porous and hard
		K_2MnO_4	04-010-3595	***$K_2Si_2O_5$***	(s)	
		$MnSiO_3$	04-013-3698	SiO_2	(slag)	
		$Mn_{0.95}O$	04-002-8161	K_2O	(slag)	
				KOH	(g)	
				Mn_2O_3	(ss1)	
				K	(g)	
	Inert	***K_2SiO_3***	00-031-1076	$Mn_3O_4^{()(+)(2-)}$	(ss1)	Black stone-hard
		$K_2Si_4O_9$	00-030-0978	***$K_2Si_2O_5$***	(s)	
		K_2MnO_4	04-010-3595	SiO_2	(slag)	
		Mn_7SiO_{12}	00-033-0904	K_2O	(slag)	
		SiO_2	00-046-1045	MnO	(slag)	
		$MnSiO_3$	04-013-3698			

MnSiTi	Oxidising	***$K_2Ti_4O_9$***	01-083-2764	K_2O	(slag)	Black stone-hard
		K_4SiO_9	04-010-7078	SiO_2	(slag)	
		K_2MnO_4	04-010-3595	$Mn_3O_4^{()(+)(2-)}$	(ss1)	
		SiO_2	01-079-0446	***K_2SiO_3***	(s)	
		$TiO_{0.84}$	04-006-1902	TiO_2	(slag)	
		$Ti_{0.9}Mn_{2.1}O_4$	04-008-0323	MnO	(slag)	
	Reducing	***$K_2Ti_2O_5$***	04-012-6258	MnO	(ss1)	Black stone-hard
		K_2SiO_3	00-031-1076	***K_2SiO_3***	(s)	
		K_2MnO_4	04-010-3595	K_2O	(slag)	
		$K_2TiSi_6O_{15}$	00-040-0483	KOH	(g)	
		Mn_2O_3	04-005-4578	TiO_2	(slag)	
		SiO_2	00-046-1045	SiO_2	(slag)	
		TiO_2	04-005-4661	$(KOH)_2$	(g)	
		$MnTiO_3$	04-006-6623	K	(g)	
	Inert	***K_2MnO_4***	04-001-3595	K_2O	(slag)	Black and hard
		$K_2Ti_2O_3$	00-001-1016	SiO_2	(slag)	
		K_2SiO_9	04-011-6870	$Mn_3O_4^{()(+)(2-)}$	(ss1)	
		SiO_2	00-046-1045	***K_2SiO_3***	(s)	
		$TiMnO_3$	04-015-9607	TiO_2	(slag)	
				MnO	(slag)	
				K	(g)	
MnFe	Oxidising	***$KFeO_2$***	04-013-8446	K_2O_2	(s)	Black and partially stone-hard
		K_2FeO_4	00-025-0652	Fe_2O_3	(ss1)	
		K_2MnO_4	00-012-0264	Mn_2O_3	(ss1)	
		Mn_2O_3	04-005-4578	K	(g)	
		Fe_2O_3	00-039-1346	KO	(g)	
	Reducing	***$KFeO_2$***	04-013-8446	KOH	(g)	Green black stone-hard
		$(FeO)_{0.099}(MnO)_{0.901}$	01-077-2362	MnO	(ss1)	
		FeO	01-089-2468	FeO	(ss1)	
		MnO	00-006-0592	$(KOH)_2$	(g)	
				K	(g)	
	Inert	***$KFeO_2$***	04-013-8446	K_2O	(slag)	Black, hard lumps within a cake
		K_2MnO_4	00-012-0264	$MnFe_2O_4^{()(2-)}$	(ss1)	
		Mn_3O_4	00-024-0734	$Mn_3O_4^{()(2+)(2-)}$	(ss1)	
				Fe_2O_3	(slag)	
				K	(g)	
				Mn_2O_3	(slag)	
				MnO	(slag)	
				$Fe_3O_4^{(+)()}$	(ss1)	
				$FeMn_2O_4^{(+)(3-)(-)()}$	(ss1)	
				KO	(g)	

MnFeAl	Oxidising	***$KFeO_2$***	04-013-8446	***$KAlO_2$***	(s)	Black with green-yellow particles. Hard surface
		$KAlO_2$	04-008-6553	K_2O_2	(l)	
		K_2FeO_4	04-007-6781	Fe_2O_3	(ss1)	
		K_2MnO_4	00-012-0264	Mn_2O_3	(ss1)	
		$FeAl_2O_4$	00-034-0192	K	(g)	
		$MnAl_2O_4$	00-029-0338	KO	(g)	
	Reducing	***$KFeO_2$***	04-013-8446	KOH	(g)	Dark brown. Powder with lumps
		$KAlO_2$	04-008-6553	***$KAlO_2$***	(s)	
		$(FeO)_{0.099}(MnO)_{0.901}$	01-077-2362	FeO	(ss1)	
		$MnAl_2O_4$	04-014-4791	MnO	(ss1)	
		$Fe_{0.8}Al_{1.2}O_3$	04-016-2652	Fe_2O_3	(ss1)	
		Al_2O_3	00-056-1186	$(KOH)_2$	(g)	
		MnO	04-005-4310	$Fe_3O_4^{(+)(-)()(-)}$	(ss2)	
				K	(g)	
				$FeAl_2O_4^{(+)}$	(ss2)	
	Inert	***K_3FeO_2***	00-048-0957	***$KAlO_2$***	(s)	Black, lumps within the cake
		$KFeO_2$	04-013-8446	K_2O	(slag)	
		$KAlO_2$	04-008-6553	Fe_2O_3	(slag)	
		Mn_3O_4	00-002-1062	$FeMn_2O_4^{(-)(+)}$	(ss1)	
		$MnAl_2O_4$	04-014-4791	K	(g)	
				$Fe_3O_4^{(+)}$	(ss1)	
				Mn_2O_3	(slag)	
				$Mn_3O_4^{()(2-)}$	(ss1)	
				MnO	(slag)	
				FeO	(slag)	
				Al_2O_3	(slag)	
				KO	(g)	

3.2.1. Phase Composition

The samples showed significant visual changes after exposure. Formation of stone hard or lumpy compounds along with black or green colour was observed. XRD showed that eight interacted compounds were formed for MnSi summarised over all investigated environments. The other oxygen carriers formed ten interacted compounds for MnSiTi, six for MnFe and nine for MnFeAl. After exposure with potassium carbonate the silica-containing oxygen carriers showed agglomerating properties to greater extent compared to iron-containing oxygen carriers. This is mainly a result from formation of alkali silicates. The potassium also reacted with titanium to some extent according to XRD, which might contribute to some agglomeration. The oxygen carriers not containing silica or titanium showed less tendency to agglomerate.

After exposure with potassium in oxidising environment, the particles showed changes in shape as well as changes in composition, which could be associated with melt formation or the pre-treatment of grinding. Similar results were found for the two additional exposures.

Elemental mapping on cross section of MnSiTi after exposure in reducing environment showed that potassium penetrated the oxygen carrier and was detected across the whole cross section, see Figure 3. Additionally, clusters of oxygen carriers can be found together with potassium across the sample. XRD detected potassium silicates and compounds such as K_2MnO_4 and $K_2Ti_2O_3$ indicating interaction. These compounds have likely formed in or on the outside of the oxygen carrier. Figure 3 show that oxygen carriers become larger and change form due to sticking together as a result from interacting with potassium.

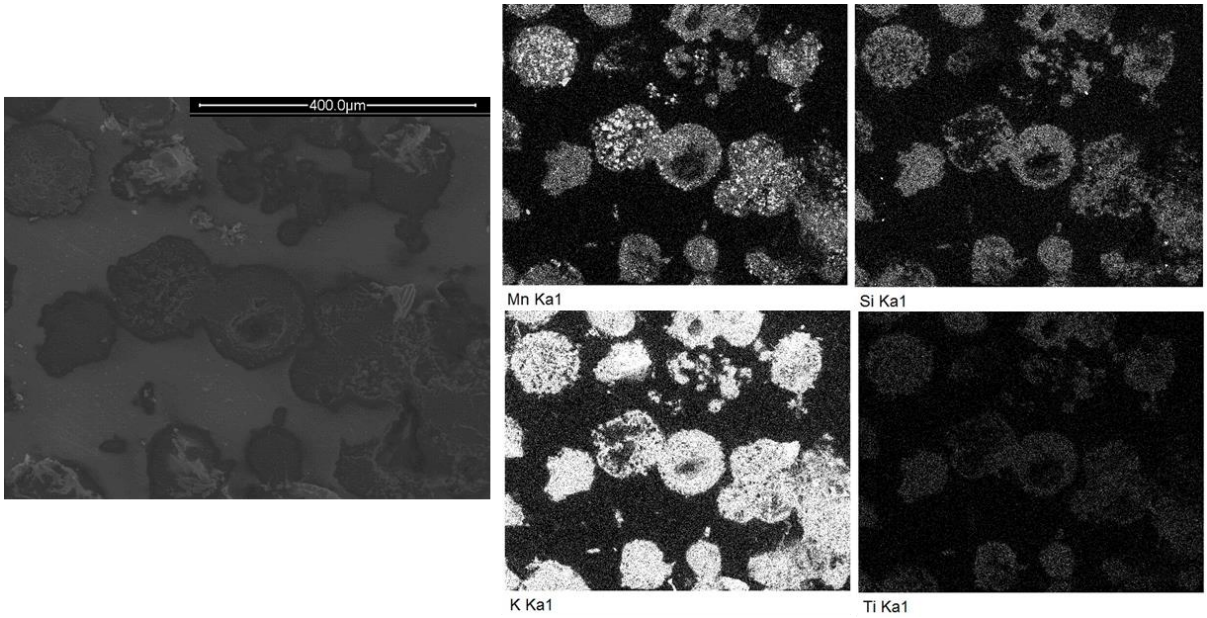

Figure 3 Cross section analysis after exposure of MnSiTi in reducing environment with potassium. Elemental mapping in the two right columns.

Both MnSiTi and MnSi formed stone-hard samples, which was noticed for all exposure environments. Results indicates that, for oxygen carriers containing silicon, potassium will stick to and react at the surface and the original spherical shape will not be preserved during exposure.

The oxygen carrier MnFe formed a black stone-hard cake in inert and oxidising environment while a green stone-hard cake was found for reducing exposure. The difference in colour between the exposures is likely due to the formation of MnO which only forms in reducing environment. One interacted compound, $KFeO_2$, was detected by XRD after reducing exposure which apparently has a large impact on agglomeration. From SEM-EDX images after both oxidising and reducing environments, it was difficult to distinguish individual potassium ash component from the MnFe oxygen carrier particles. As an example, elemental mapping of MnFe after reducing exposure is presented in Figure 4. This cross-section analysis showed that potassium had been absorbed on to the oxygen carriers, and many oxygen carrier particles could be found together in an agglomerate. Thus, it is likely that potassium carbonate had melted during exposure pulling the oxygen carriers closer together.

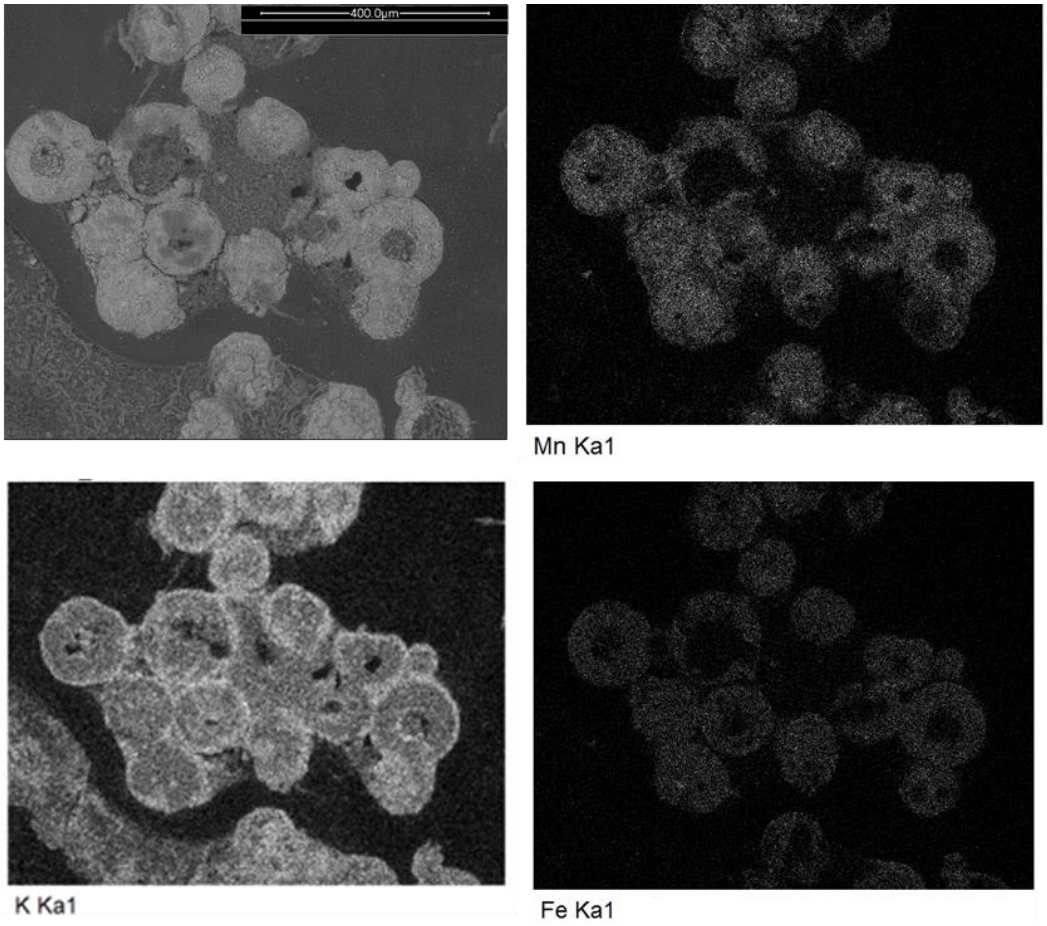

Figure 4 Cross section analysis after exposure of MnFe in oxidising environment with potassium. With elemental mapping of manganese (top right), potassium (bottom left) and iron (bottom right).

3.2.2. Thermodynamic Calculations

Thermodynamic calculations showed formation of phases including species from both ash and oxygen carrier in all investigated cases except for MnFe which predicted none. Calculations for MnSi, MnSiTi and MnFeAl predicted three interacted compounds in total for all investigated environments. One important outcome from the thermodynamic calculations is the formation of gaseous potassium and slag phases. Since gas composition was not monitored during exposure it is possible that some potassium evaporated and either reacted with the oxygen carrier or exited as gas. Formation of slag phase have possibly contributed to agglomeration, as discussed related to Figure 4. It is likely that amorphous phases have been formed which are not detectable by XRD.

Large inconsistencies were found among all thermodynamic calculations and XRD results. Most probably this depends on the formation of amorphous phases and non-compatibility between XRD and FactSage databases. For MnFe no interacted compounds were predicted by FactSage while XRD found compounds such as $KFeO_2$, K_3FeO_4 and K_2MnO_4. Closer investigation showed that these compounds are not present in any of the databases. The databases have not been optimised for systems including potassium. This is probably the main reason for the diverse results and why the calculations did not predict interaction in some cases.

Another finding is that Table 3 predicts $KAlO_2$ in all three environments for MnFeAl. A phase diagram for MnFeAl was created in FactSage. The phase diagram showed interaction between aluminium and potassium. For each investigated partial oxygen pressure ($log_{10}p(O_2)$ between 0 and -15 atm.) and oxygen carrier to ash ratio (between 0 and 1) formation of $KAlO_2$ was noticed in each region, indicating a stable compound. Thermodynamically, potassium is more likely to form compounds with aluminium when both aluminium, manganese and iron are present. This is beneficial as samples which reacted to form K_2MnO_4 agglomerated to a higher extent while this compound was not found for MnFeAl and these samples did not show the same agglomerating behaviour. Thus, aluminium containing oxygen carrier may have some advantages regarding agglomeration, due to formation of $KAlO_2$ which gives a stable oxygen carrier.

3.3. Interactions with dicalcium phosphate

Results for exposure processes including dicalcium phosphate are gathered in Table 4. The table gives an overview of the XRD and FactSage results as well as the visual observation of the sample after exposure.

Table 4 Summarised results for exposures carried out with dicalcium phosphate. Interaction between the ash component and oxygen carrier in italic and bold text.

Oxygen carrier		**XRD**		**FactSage**		**Visual**
		Compound	**PDF No**			
MnSi	Oxidising	***$Ca_{19}Mn_2(PO_4)_{14}$***	00-048-1193	$Ca_3P_2O_8$	(s)	Grey-white powder
		Mn_7SiO_{12}	00-033-0904	SiO_2	(s)	
		SiO_2	00-046-1045	***$Mn_3(PO_4)_2$***	(s)	
		$Ca_2P_2O_7$	00-009-3876	Mn_7SiO_{12}	(ss1)	
	Reducing	***$Ca_{19}Mn_2(PO_4)_{14}$***	00-048-1193	$Ca_3P_2O_8$	(s)	White cake
		SiO_2	00-046-1045	***$Mn_3(PO_4)_2$***	(s)	
		Mn_2O_3	04-005-4578	$MnSiO_3$	(ss1)	
		$CaSiO_3$	00-066-0271	SiO_2	(s)	
				$CaSiO_3$	(ss1)	
	Inert	***$Ca_{19}Mn_2(PO_4)_{14}$***	00-048-1193	$Ca_3P_2O_8$	(s)	Grey-white powder with some lumps
		$Mn_3(PO_4)_2$	00-040-0112	SiO_2	(s)	
		Ca_2SiO_4	00-023-1043	***$Mn_3(PO_4)_2$***	(s)	
		$CaSiO_3$	00-066-0271	Mn_7SiO_{12}	(ss1)	
		SiO_2	00-046-1045			
		$Ca_2P_2O_7$	00-009-3876			
		CaO	00-043-1001			
MnSiTi	Oxidising	***$Ca_{19}Mn_2(PO_4)_{14}$***	00-048-1193	SiO_2	(s)	Grey-white powder with lumps
		$CaMnTi_2O_6$	00-066-0325	$Ca_3(PO_4)_2$	(s)	
		$Ca_2P_2O_7$	04-009-3876	TiO_2	(ss1)	
		SiO_2	00-046-1045	Mn_7SiO_{12}	(ss2)	
		TiO_2	04-005-4661	***$Mn_3(PO_4)_2$***	(s)	
	Reducing	***$Ca_{19}Mn_2(PO_4)_{14}$***	00-048-1193	$MnSiO_3$	(ss1)	White and
		$MnTiO_3$	04-007-4402	$Ca_3(PO_4)_2$	(s)	

		SiO_2 TiO_2 CaO	00-046-1045 04-005-4661 00-043-1001	***$Mn_3(PO_4)_2$*** $MnTiO_3$ ***$CaSiTiO_5$*** ***$CaSiO_3$***	(s) (ss2) (s) (ss1)	yellow cake
	Inert	***$Ca_{19}Mn_2(PO_4)_{14}$*** ***$CaSiO_3$*** ***$CaTiO_3$*** ***Mn_7SiO_{12}*** ***Ca_3SiO_5*** ***$Ti_4(PO_4)_3O_3$*** $MnSiO_3$ TiO_2 Mn_2O_3 $Ca_4O(PO_4)_2$ $Ca_2P_2O_7$	00-048-1193 00-066-0271 04-018-8646 00-033-0904 00-055-0738 04-015-7753 04-013-3698 04-005-4661 04-005-4578 00-025-1137 00-009-3876	$Ca_3(PO_4)_2$ $MnSiO_3$ ***$Mn_3(PO_4)_2$*** ***$CaSiTiO_5$*** ***$CaSiO_3$*** Mn_7SiO_{12}	(s) (ss1) (s) (s) (ss1) (ss2)	Grey-white powder with some lumps
MnFe	Oxidising	***$Ca_9Fe(PO_4)_7$*** ***$Ca_{19}Mn_2(PO_4)_{14}$*** $Ca_2P_2O_7$ Mn_2O_3 Fe_2O_3	00-045-0338 00-048-1193 04-009-3876 04-005-4578 00-039-0238	Fe_2O_3 $Ca_3(PO_4)_2$ Mn_2O_3 ***$Mn_3(PO_4)_2$***	(ss1) (s) (ss1) (s)	Grey white powder with lumps
	Reducing	***$Ca_{9.33}Fe_{1.167}(PO_4)_7$*** ***$Ca_{19}Mn_2(PO_4)_{14}$*** $(FeO)_{0.331}(MnO)_{0.669}$ FeO CaO Fe_2O_3	01-072-6760 00-048-1193 01-077-2360 01-089-2468 00-043-1001 00-039-1346	FeO MnO $Ca_3(PO_4)_2$ ***$Mn_3(PO_4)_2$*** Fe_2O_3 CaO	(ss1) (ss1) (s) (s) (ss1) (ss1)	Grey with hard lumps
	Inert	***$Ca_9Fe(PO_4)_7$*** $Fe_{2.47}Mn_{0.53}O_4$ CaO Fe_2O_3 $Ca_2P_2O_7$	00-045-0338 04-002-9145 00-043-1001 00-039-1346 04-009-3876	$Ca_3(PO_4)_2$ Fe_2O_3 Mn_2O_3 ***$Mn_3(PO_4)_2$***	(s) (ss1) (ss1) (s)	Grey-white powder with some lumps
MnFeAl	Oxidising	***$Ca_9Al(PO_4)_7$*** ***$Ca_{19}Mn_2(PO_4)_{14}$*** $Ca_2P_2O_7$ $AlFe_2O_4$ Mn_2AlO_4 Fe_2O_3	00-048-1192 00-048-1193 00-009-0346 01-089-7408 00-029-0881 00-005-0637	Al_2O_3 $Ca_3(PO_4)_2$ Fe_2O_3 ***$Mn_3(PO_4)_2$*** ***$AlPO_4$***	(ss1) (s) (s) (s) (ss1)	Grey-white powder
	Reducing	***$Ca_9Fe(PO_4)_7$*** ***$Ca_9Al(PO_4)_7$*** ***$Ca_{19}Mn_2(PO_4)_{14}$*** $Ca_2P_2O_7$ $AlFe_2O_4$	00-045-0338 00-048-1192 00-048-1193 00-009-0346 01-089-7408	$FeAl_2O_4$ $Ca_3(PO_4)_2$ ***$Mn_3(PO_4)_2$*** ***$Fe_{10}P_6O_{26}$*** $MnAl_2O_4$	(ss1) (s) (s) (s) (ss1)	Grey with hard lumps

		Mn_2O_3 Fe_2O_3	04-005-4578 00-039-1346	$Fe_3O_4^{(2-)()(-)(+)}$ $MnFe_2O_4^{()(2-)}$ $FeMn_2O_4^{(-)(2-)}$	(ss2) (ss2) (ss2)	
	Inert	***$Ca_9Fe(PO_4)_7$*** ***$Ca_{19}Mn_2(PO_4)_{14}$*** $MnFeAlO_4$ Fe_2O_3 Mn_2O_3 $Ca_2P_2O_7$	00-045-0338 00-048-1193 04-005-9715 00-039-1346 04-005-4578 04-009-3876	Al_2O_3 $Ca_3(PO_4)_2$ Fe_2O_3 ***$Mn_3(PO_4)_2$*** ***$AlPO_4$*** $MnFe_2O_4^{()(2-)}$ $FeMn_2O_4^{(-)(2-)}$	(ss1) (s) (ss1) (ss1) (s) (ss2) (ss2)	Grey-white powder with some lumps

3.3.1. Phase Composition

In contrast to the samples exposed to potassium, no stone hard samples were found with dicalcium phosphate. After exposure most samples became grey and consisted of powder including lumps. XRD-analysis showed that $Ca_2P_2O_7$, which forms during heat up, was found in all samples exposed to calcium phosphate in both inert and oxidising environment. These samples did not show drastic visual changes indicating that the compound $Ca_2P_2O_7$ is stable during these conditions. XRD showed that seven interacted compounds were formed for MnSi summarised over all investigated environments. The other oxygen carriers formed nine interacted compounds for MnSiTi, five for MnFe and seven for MnFeAl. Compared to solely carbon carbonate exposure more interacted compounds are detected when adding phosphorous.

Calcium did not react with MnFe after any exposure with calcium carbonate, but in presence of phosphorous, a surface layer was formed including both calcium and phosphorous. Figure 5 shows a very clear surface layer consisting of both calcium and phosphorous for MnFe. It is possible that phosphorous drags calcium to the MnFe surface which then sticks to it.

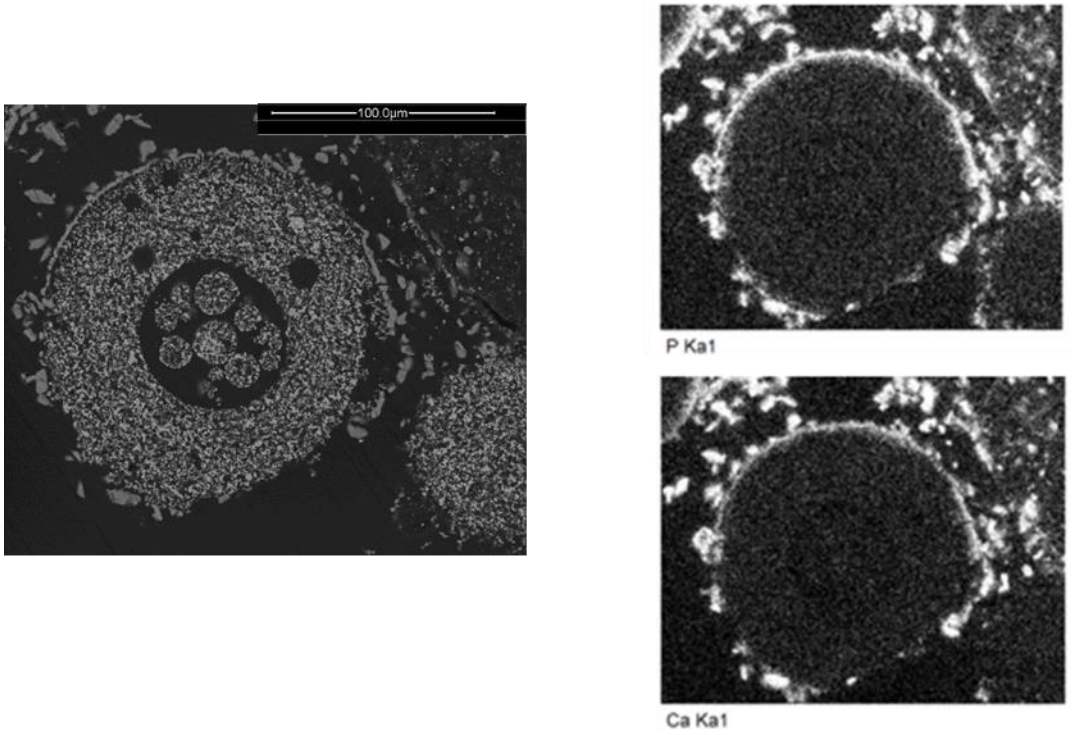

Figure 5 Cross section analysis after exposure of MnFe in reducing environment with dicalcium phosphate. Electron image to the left and element mapping of phosphorous (top right) and calcium (bottom right).

MnFeAl did not form a stone hard cake in any case, however it changed colour and/or formed lumps depending on the environment and ash component. Different results were obtained compared to other oxygen carriers. Calcium was found in the middle of the oxygen carrier particle, due to the hollow core formed during production, but also surrounding the oxygen carrier as in Figure 6. The surface layer formed around the particle contained more phosphorous and less calcium compared to the rest of the oxygen carriers. Point analyses were performed on points inside the particle and on the outer part of the particle. These showed an increase of phosphorous content, from approximately three percent inside to seventeen percent on the phosphorous layer formed around the particles. It is possible that the aluminium content in MnFeAl hindered calcium to stick to the particle surface.

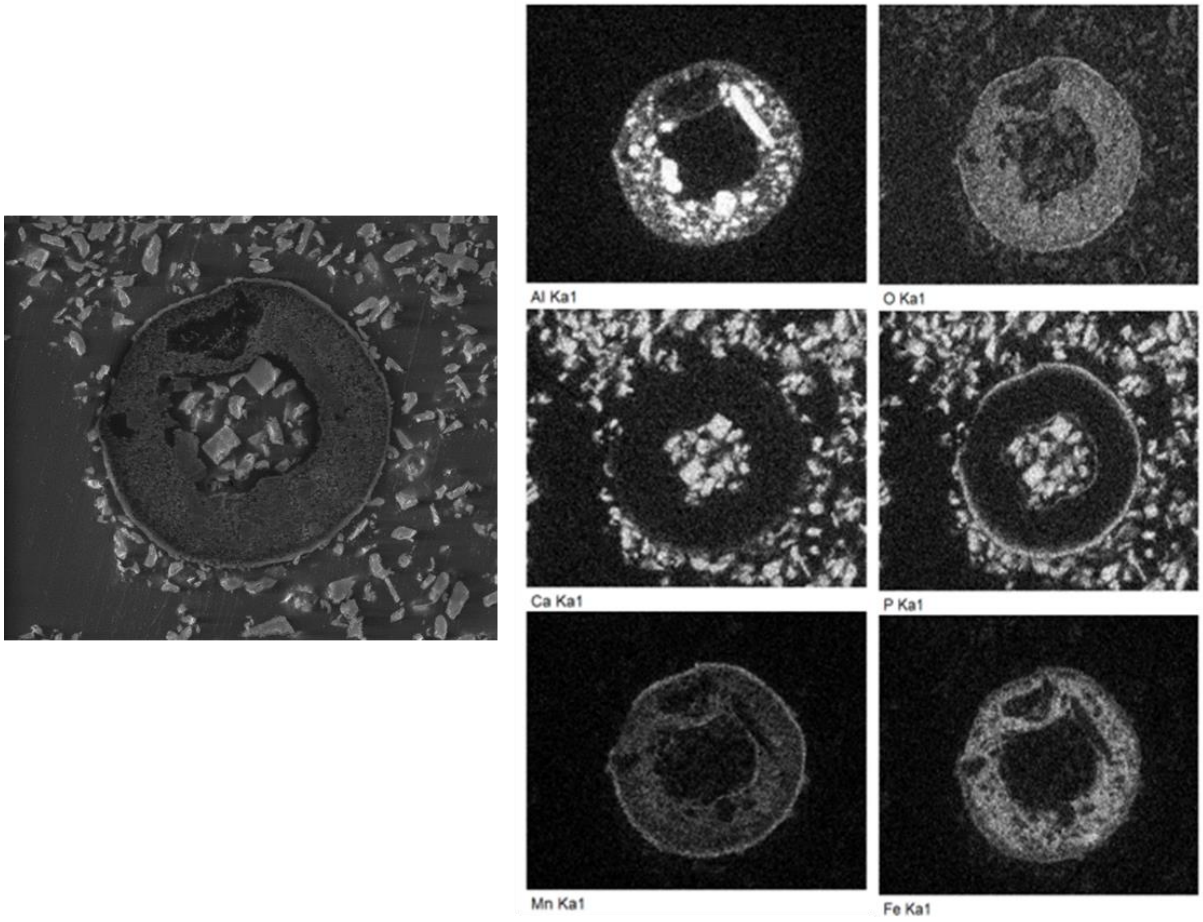

Figure 6 Cross section analysis of MnFeAl after exposure with dicalcium phosphate in reducing environment. With the electron image on the left and element mapping in the two right columns.

After exposure with the silicon containing oxygen carriers, the samples were still powders containing harder lumps. In the reducing environment the samples became white while they remained grey and white in the other environments. Exposure with only calcium itself did not interact with MnSiTi, as discussed above and shown in Table 2. However, in presence of phosphorous it was shown to have other properties. Phosphorous and calcium together formed a surface layer around the oxygen carrier keeping the interior intact in form and composition as seen in Figure 7.

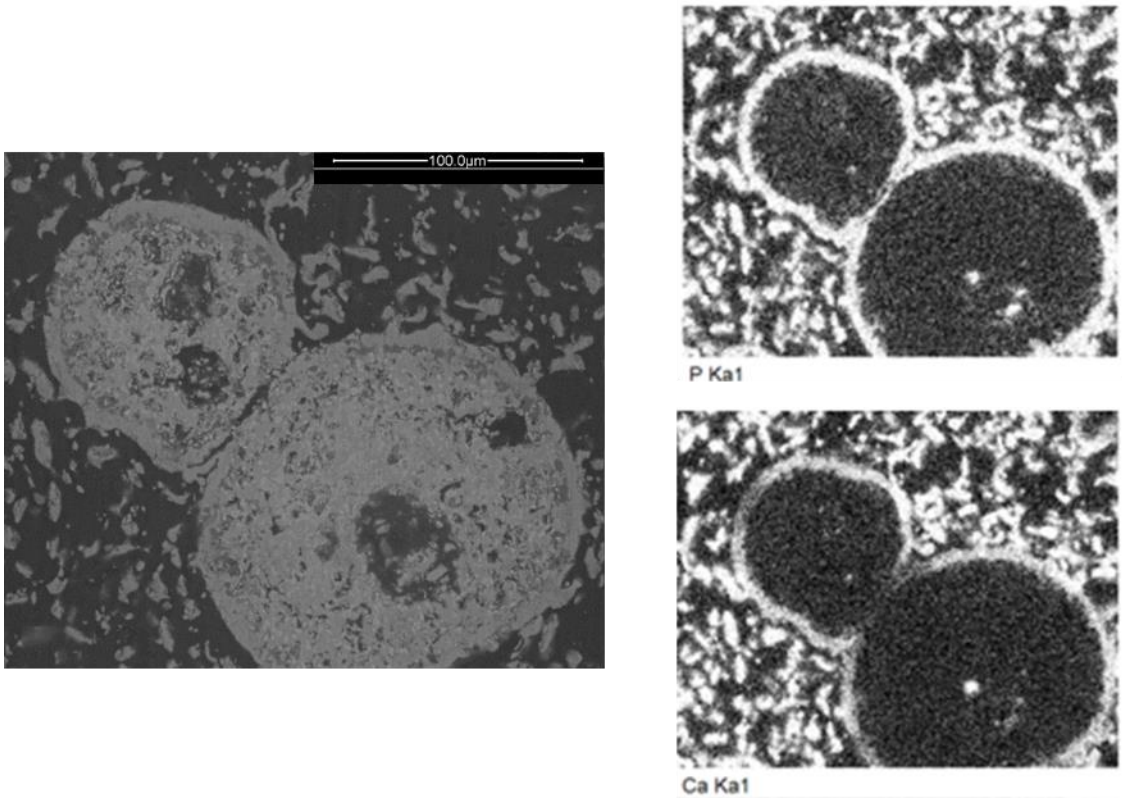

Figure 7 Cross section analysis of MnSiTi after exposure with dicalcium phosphate in reducing environment. With the electron image on the left and element mapping of phosphorous (top right) and calcium (bottom right).

3.3.2. Thermodynamic Calculations

Thermodynamic calculations showed formation of phases including species from both ash and oxygen carrier in all investigated cases. Calculations for MnSi predicted four interacted compounds in total for all investigated environments. The other oxygen carriers formed seven for MnSiTi, three for MnFe and six for MnFeAl. The number of interacted compounds is relatively well aligned with the findings by XRD which found a higher number of interacted compounds. This investigated system is the largest one in this study including five components Mn-Fe-Al-Ca-P. There are several factors that could affect these results. Thermodynamic calculations assume that all compounds are perfectly mixed. As evident from Figure 5, Figure 6 and Figure 7 a surface layer is formed around the oxygen carriers resulting in a concentration gradient which is not taken into account during calculations.

At higher temperatures dicalcium phosphate will form dicalcium diphosphate thermodynamically. Table 4 indicates the formation of $Ca_2P_2O_7$ while thermodynamic calculations predicts formation of $Ca_3P_2O_8$. Even though $Ca_2P_2O_7$ is included in the FToxid database the Ca-P-Si-O system has been optimised including $Ca_3P_2O_8$ which is a possible explanation for this result.

4. Discussion

In real CLC processes the oxygen carriers will endure fluidisation, different temperature gradients, velocities and environments. By utilising fixed bed condition, as done in the present investigation, more contact and extensive time of contact can be achieved in comparison to a

fluidised bed. Oxygen carriers endure a reducing environment in the fuel reactor. This is also where the oxygen carriers first come in contact with the ash and therefore the most interesting case to investigate. The reaction paths for the ash compounds may vary considerably and be composed of several steps. Some compounds may interact with the oxygen carrier after evaporating or interacting with another compound. For example, potassium is likely to form KCl (if chlorine is present) or KOH in the gas phase, which thereafter may come in contact with the oxygen carriers with further reactions possible. There may also be some solid-solid reactions between ash and oxygen carriers, but it is possible that the compounds used in the present study may not be the actual reacting species. However, by using solid carbonate and phosphate compounds the reaction mechanism is simplified and one aspect of the possible interaction is investigated. Below follows some discussions of the results found in this study.

4.1. Thermodynamic calculations

Results from FactSage show that interaction can be expected in all exposures. For silicates and oxides, the database FToxid is the most comprehensive one and therefore used in the calculations [42]. The major system, which includes aluminium, calcium, iron, magnesium and silicone has been optimised, although not for all binary or ternary systems. Addition of potassium in these calculations may therefore result in some uncertainties [43]. This is evident from the summarising tables as calculations for exposures with potassium were the ones which deviated the most.

In addition to lack of data, lack of prediction could be due to kinetic and mass transfer factors. To reach thermodynamic equilibrium, the system requires a large amount of time. Six hours exposure may not be enough for the system to reach equilibrium which can result in intermediate products being formed and found when analysed. Chemical reactions naturally occur with different rates which also affects the final composition of the solids. Fast reactions may for example deplete reactants hindering formation of products for the slower reaction.

It is also important to keep in mind during what circumstances the thermodynamic calculations are performed. The calculations were performed for equal amount of oxygen carrier and ash compound evenly exposed to the same environment. During exposure however, since the sample is contained in a ceramic boat the top surface will be exposed to the current environment while the content inside the boat will be exposed to a gradient of this environment. It is also possible that some small areas inside these samples are enriched in ash compound which may influence the results further. For thermodynamic calculations the molar ratio between compounds is important with respect to which compounds are thermodynamically stable. Considering this, it may be more reasonable to analyse phase stability in different regions of different oxygen partial pressures and molar ratios to get the most reliable result.

During CLC operation, manganese transfers its oxygen through a series of phase changes, i.e. Mn_2O_3 to Mn_3O_4 to MnO. Figure 8 shows the phase diagram of manganese under different oxygen partial pressures. The operating point for oxidising exposure at 800°C lies in between the two phases Mn_2O_3 and Mn_3O_4 which explains why Mn_2O_3 is formed in some oxidising exposures. Additionally, since oxidising exposures are cooled in oxidising environment it is possible that Mn_2O_3 formed during cooling which then may have interacted with other

compounds. It is expected that in a system operated isothermally at temperatures above 900°C, the phase change will be between Mn_2O_3 and Mn_3O_4.

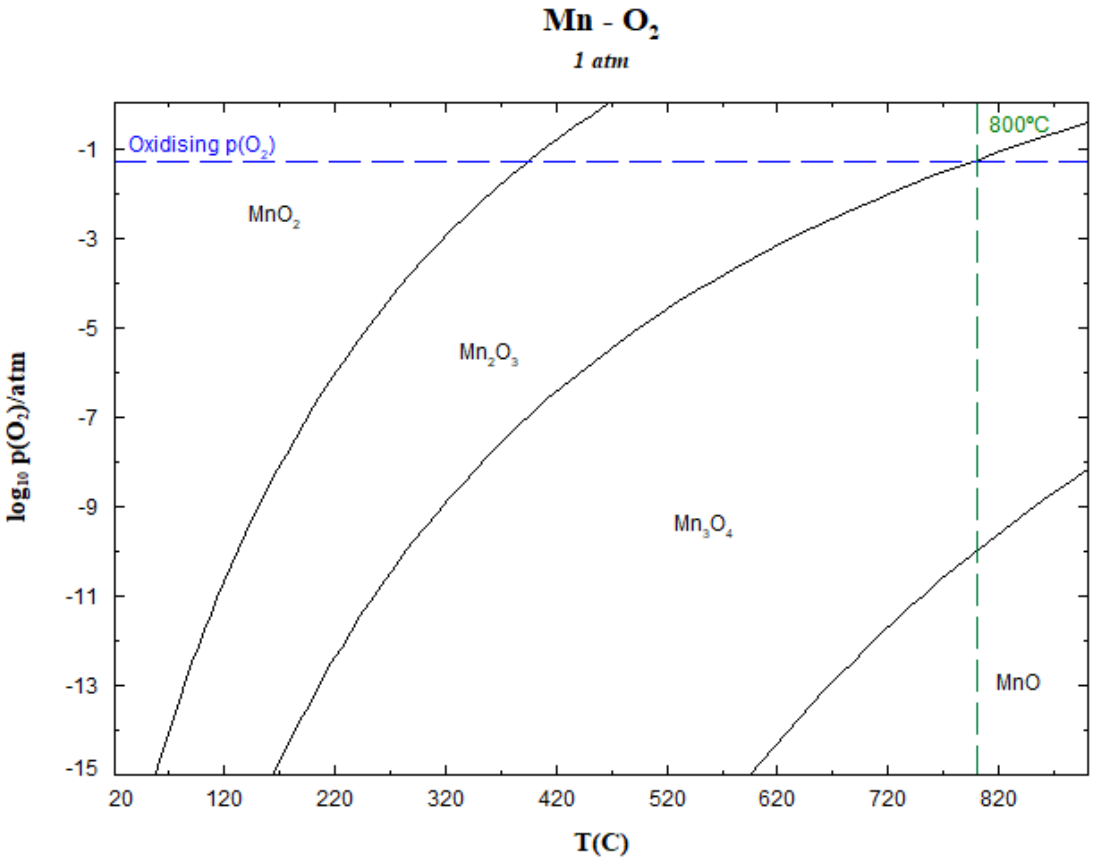

Figure 8 Phase diagram for manganese under different oxygen partial pressures. Operating point for oxidising exposure indicated at the intersection.

4.2. Morphology and phase composition

Holes and cracks could be seen on the oxygen carrier particles in some SEM images. For example, absorption of ash compounds clearly changed the appearance of the spheres. Cracking of surfaces could be observed for other cases as well which may have been caused by diffusion and reaction of the ash components. If an ash component sticks to the surface it can affect the particle in several ways. It may diffuse into the particle, leading to cracks or deformation, depending upon the chemical reaction. If reaction occurs after or during diffusion where for example the carbonate or ash components leaves in the gas phase it could affect the physical shape of the particles. Lastly, reaction may also occur on the surface before diffusion leading to cracks and holes in the oxygen carrier particle. These types of phenomena could have serious consequences on oxygen carrier performance, i.e. reactivity and attrition behaviour.

Almost all exposures with potassium resulted in formation of a stone hard cake, and hence likely the most problematic compound with respect to biomass combustion in CLC. Oxygen carriers containing silicon seemed to agglomerate more easily when in contact with potassium. Previous studies have shown that silicon, potassium and calcium accumulate in the bed during

biomass combustion when using manganese ores as bed material [21, 35]. The samples exposed with potassium were porous in some cases and could be a result of evaporation of volatile species.

For each oxygen carrier, with the exception MnFeAl in reducing and inert environment, K_2MnO_4 was detected by XRD. For both MnFe and MnFeAl the crystalline phase $KFeO_2$ was detected in all environments. Even though FactSage did not thermodynamically predict the compound $KFeO_2$, by comparing samples after exposure, it is possible that $KFeO_2$ was not formed to the same extent when aluminium was present. After exposure in reducing environment, MnFe agglomerated heavily, similar to Figure 4, while MnFeAl only had a few lumps. This may further be explained by the absorption of potassium in the case with MnFeAl which formed $KAlO_2$. It is possible that $KAlO_2$ provides stability to the oxygen carrier. Ndlela, S.C and Shanks, B.H. investigated reduction behaviour of potassium promoted iron oxide under mixed steam and hydrogen atmospheres. It was found that potassium incorporation stabilises the iron oxide against reduction by forming $KFeO_2$, which might be the case here [44].

The actual fate of alkali in CLC can be discussed and may not be so straightforward. By absorption of alkali in the bed material it may lead to deactivation of the bed, defluidisation, shorter lifetime and a need to change bed material more often. In this case it is important that the bed material is relatively cheap. On the other hand, if potassium evaporates it may save some cost regarding the bed material but further on in the process these gases may lead to corrosion and fouling on heat transfer surfaces, leading to even larger expenses. One way to work around these problems could be to use bed materials with the tendency to absorb the alkali but not form agglomerates. Thus, the bed properties will be preserved, and the alkali released in the gas phase limited. On the other hand, absorption of alkali might shorten oxygen carrier lifetime. For example, formation of slag phases and interaction between MnSi or MnSiTi and potassium which formed $K_xS_yO_z$ could reduce oxygen carrier lifetime. A lifetime reduction will impose a need for more frequent renewal of bed material which can only be economically feasible for low cost oxygen carriers.

5. Conclusions

This study showed that manganese-based oxygen carriers and ash species react to different extents with different implications with respect to physical behaviour. The main conclusions of this study are,

- Exposures of oxygen carriers with calcium carbonate showed the formation of some interacted compounds, however there was no sign of severe agglomeration for any oxygen carrier.
- Exposures showed that potassium contributes to agglomeration independent of oxygen carrier type and environment. Particles containing silicon agglomerated to greater extent while particles including iron were more stable. Additionally, MnFeAl did not show as severely agglomerated samples compared to the other oxygen carriers which is likely due to the aluminium content.
- Dicalcium phosphate was showed to form a coating on the particle surfaces.

- Some inconsistencies between thermodynamic predictions and experimental results is observed. This may be explained by lack of information in the used databases and that all systems and subsystems are not optimised, and further optimisation related to manganese rich systems should be performed.

Acknowledgements

The authors acknowledge the work of the late Dongmei Zhao (deceased Dec 18, 2016). At the time of her death, she was closely involved with this research and made many important contributions. This work was financed by Formas, the Swedish Research Council for Environment, Agricultural Sciences and Spatial Planning (2014-918).

References

[1] Fuss S, Canadell JG, Peters GP, Tavoni M, Andrew RM, Ciais P, et al. Betting on negative emissions. Nature Climate Change. 2014;4:850.

[2] IPCC. Climate Change 2014: Mitigation of Climate Change. Contribution of Working Group III to the Fifth Assessment Report of the Intergovernmental Panel on Climate Change. In: Edenhofer O, Pichs-Madruga R, Sokona Y, Farahani E, Kadner S, Seyboth K, et al., editors. Cambridge, United Kingdom and New York, USA2014.

[3] Gasser T, Guivarch C, Tachiiri K, Jones CD, Ciais P. Negative emissions physically needed to keep global warming below 2°C. Nature Communications. 2015;6.

[4] Azar C, Lindgren K, Obersteiner M, Riahi K, van Vuuren DP, den Elzen KMGJ, et al. The feasibility of low CO2 concentration targets and the role of bio-energy with carbon capture and storage (BECCS). Climatic Change. 2010;100:195-202.

[5] Lyngfelt A. Oxygen carriers for chemical-looping combustion. In: Fennell P, Anthony B, editors. Calcium and Chemical Looping Technology for Power Generation and Carbon Dioxide (CO2) Capture. 1st ed: Woodhead Publishing; 2015. p. 221-54.

[6] Adanez J, Abad A, Garcia-Labiano F, Gayan P, de Diego LF. Progress in Chemical-Looping Combustion and Reforming technologies. Progress in Energy and Combustion Science. 2012;38:215-82.

[7] Lyngfelt A. Chemical-looping combustion of solid fuels - Status of development. Applied Energy. 2014;113:1869-73.

[8] Leion H, Mattisson T, Lyngfelt A. The use of petroleum coke as fuel in chemical-looping combustion. Fuel. 2007;86:1947-58.

[9] Mattisson T, Lyngfelt A, Leion H. Chemical-looping with oxygen uncoupling for combustion of solid fuels. International Journal of Greenhouse Gas Control. 2009;3:11-9.

[10] Rydén M, Leion H, Mattisson T, Lyngfelt A. Combined oxides as oxygen-carrier material for chemical-looping with oxygen uncoupling. Applied Energy. 2013;113:1924-32.

[11] Shulman A, Cleverstam E, Mattisson T, Lyngfelt A. Manganese/Iron, Manganese/Nickel, and Manganese/Silicon Oxides Used in Chemical-Looping With Oxygen Uncoupling (CLOU) for Combustion of Methane. Energy & Fuels. 2009;23:5269-75.

[12] Azimi G, Leion H, Rydén M, Mattisson T, Lyngfelt A. Investigation of different Mn-Fe oxides as oxygen carrier for chemical-looping with oxygen uncoupling (CLOU). Energy and Fuels. 2013;27:367-77.

[13] Jing D, Arjmand M, Mattisson T, Rydén M, Snijkers F, Leion H, et al. Examination of oxygen uncoupling behaviour and reactivity towards methane for manganese silicate oxygen carriers in chemical-looping combustion. International Journal of Greenhouse Gas Control. 2014;29:70-81.

[14] Mattisson T, Jing D, Azimi G, Rydén M, Van Noyen J, Lyngfelt A. Using $(Mn_xFe_{1-x})_2SiO_5$ as oxygen carriers for chemical-looping with oxygen uncoupling (CLOU). Presented at AIChE Annual Meeting November 3-8, San Fransisco 2013. 2013.

[15] Rydén M, Lyngfelt A, Mattisson T. Combined manganese/iron oxides as oxygen carrier for chemical looping combustion with oxygen uncoupling (CLOU) in a circulating fluidized bed reactor system. Energy Procedia. 2011;4:341-8.

[16] Pérez-Vega R, Abad A, Gayán P, de Diego LF, García-Labiano F, Adánez J. Development of (Mn0.77Fe0.23)2O3 particles as an oxygen carrier for coal combustion with CO2 capture via in-situ gasification chemical looping combustion (iG-CLC) aided by oxygen uncoupling (CLOU). Fuel Processing Technology. 2017;164:69-79.

[17] Mungse P, Saravanan G, Rayalu S, Labhsetwar N. Mixed Oxides of Iron and Manganese as Potential Low-Cost Oxygen Carriers for Chemical Looping Combustion. Energy Technology. 2015;3:856-65.

[18] Larring Y, Braley C, Pishahang M, Andreassen KA, Bredesen R. Evaluation of a mixed Fe-Mn oxide system for chemical looping combustion. Energy and Fuels. 2015;29:3438-45.
[19] Niu Y, Tan H, Hui S. Ash-related issues during biomass combustion: Alkali-induced slagging, silicate melt-induced slagging (ash fusion), agglomeration, corrosion, ash utilization, and related countermeasures. Progress in Energy and Combustion Science. 2016;52:1-61.
[20] Grimm A, Öhman M, Lindberg T, Fredriksson A, Boström D. Bed agglomeration characteristics in fluidized-bed combustion of biomass fuels using olivine as bed material. Energy and Fuels. 2012;26:4550-9.
[21] Hanning M, Gyllén A, Lind F, Rydén M. Biomass ash interactions with a manganese ore used as oxygen-carrying bed material in a 12 MWth CFB boiler. Biomass and Bioenergy. 2018;119:179-90
[22] Khan AA, de Jong W, Jansens PJ, Spliethoff H. Biomass combustion in fluidized bed boilers: Potential problems and remedies. Fuel Processing Technology. 2009;90:21-50.
[23] Gu H, Shen L, Zhong Z, Zhou Y, Liu W, Niu X, et al. Interaction between biomass ash and iron ore oxygen carrier during chemical looping combustion. Chemical Engineering Journal. 2015;277:70-8.
[24] Gatternig B, Karl J. Investigations on the mechanisms of ash-induced agglomeration in fluidized-bed combustion of biomass. Energy and Fuels. 2015;29:931-41.
[25] Hupa M. Ash-related issues in fluidized-bed combustion of biomasses: Recent research highlights. Energy and Fuels. 2012;26:4-14.
[26] Hanning M, Gyllén A, Lind F, Rydén M. Biomass ash interactions with a manganese ore used as oxygen-carrying bed material in a 12 MWth CFB boiler. Biomass and Bioenergy. 2018;119:179-90.
[27] Rubel A, Zhang Y, Liu K, Neathery J. Effect of ash on Oxygen Carriers for the application of Chemical Looping Combustion. Oil and Gas Science and Technology. 2011;66:291-300.
[28] Azis MM, Leion H, Jerndal E, Steenari BM, Mattisson T, Lyngfelt A. The Effect of Bituminous and Lignite Ash on the Performance of Ilmenite as Oxygen Carrier in Chemical-Looping Combustion. Chemical Engineering and Technology. 2013;36:1460-8.
[29] Keller M, Arjmand M, Leion H, Mattisson T. Interaction of mineral matter of coal with oxygen carriers in chemical-looping combustion (CLC). Chemical Engineering Research and Design. 2014;92:1753-70.
[30] Bao J, Li Z, Cai N. Interaction between iron-based oxygen carrier and four coal ashes during chemical looping combustion. Applied Energy. 2014;115:549-58.
[31] Ilyushechkin AY, Kochanek M, Lim S. Interactions between oxygen carriers used for chemical looping combustion and ash from brown coals. Fuel Processing Technology. 2016.
[32] Gong R, Qin C, He D, Tan L, Ran J. Oxygen Uncoupling of Cu-based Oxygen Carrier with the Presence of Coal Ash in Chemical Looping Process. Energy and Fuels. 2018;32:7708-17.
[33] Wang B, Yan R, Zhao H, Zheng Y, Liu Z, Zheng C. Investigation of chemical looping combustion of coal with CuFe 2O4 oxygen carrier. Energy and Fuels. 2011;25:3344-54.
[34] Siriwardane R, Tian H, Richards G, Simonyi T, Poston J. Chemical-looping combustion of coal with metal oxide oxygen carriers. Energy and Fuels. 2009;23:3885-92.
[35] Corcoran A, Marinkovic J, Lind F, Thunman H, Knutsson P, Seemann M. Ash properties of ilmenite used as bed material for combustion of biomass in a circulating fluidized bed boiler. Energy and Fuels. 2014;28:7672-9.
[36] Zhang S, Xiao R. Performance of iron ore oxygen carrier modified by biomass ashes in coal-fueled chemical looping combustion. Greenhouse Gases: Science and Technology. 2016;6:695-709.

[37] Källén M, Rydén M, Mattisson T, Lyngfelt A. Operation with combined oxides of manganese and silica as oxygen carriers in a 300 Wth chemical-looping combustion unit. In: Dixon T, Twinning S, Herzog H, editors. 12th International Conference on Greenhouse Gas Control Technologies, GHGT 2014: Elsevier Ltd; 2014. p. 131-9.
[38] Azimi G, Leion H, Mattisson T, Lyngfelt A. Chemical-looping with oxygen uncoupling using combined Mn-Fe oxides, testing in batch fluidized bed. Energy Procedia. 2011;4:370-7.
[39] Azimi G, Mattisson T, Leion H, Rydén M, Lyngfelt A. Comprehensive study of Mn–Fe–Al oxygen-carriers for chemical-looping with oxygen uncoupling (CLOU). International Journal of Greenhouse Gas Control. 2015;34:12-24.
[40] Strömberg B. Miljö- och förbränningsteknik - Bränslehandboken. Värmeforsk, Värmeteknisk Forskning och Arbete: Värmeforsk; 2005.
[41] Morris JD, Daood SS, Chilton S, Nimmo W. Mechanisms and mitigation of agglomeration during fluidized bed combustion of biomass: A review. Fuel. 2018;230:452-73.
[42] Bale CW, Bélisle E, Chartrand P, Decterov SA, Eriksson G, Hack K, et al. FactSage thermochemical software and databases — recent developments. CALPHAD. 2009;33:295-311.
[43] Bale CW, Bélisle E, Chartrand P, Decterov SA, Eriksson G, Gheribi AE, et al. FactSage Thermochemical Software and Databases - 2010 - 2016. Calphad. 2016;54:35-53.
[44] Ndlela SC, Shanks BH. Reduction behavior of potassium-promoted iron oxide under mixed steam/hydrogen atmospheres. Industrial and Engineering Chemistry Research. 2006;45:7427-34.